Earth and Planetary Science Letters 430 (2015) 1–8

Contents lists available at ScienceDirect

Earth and Planetary Science Letters

www.elsevier.com/locate/epsl

# Seismic anisotropy beneath the incipient Okavango rift: Implications for rifting initiation

Youqiang Yu [a], Stephen S. Gao [a], Moikwathai Moidaki [b], Cory A. Reed [a], Kelly H. Liu [a,*]

[a] Geology and Geophysics Program, Missouri University of Science and Technology, Rolla, MO 65409, USA
[b] Department of Physics, University of Botswana, Gaborone, Botswana

ARTICLE INFO

*Article history:*
Received 14 April 2015
Received in revised form 14 July 2015
Accepted 7 August 2015
Available online xxxx
Editor: B. Buffett

*Keywords:*
seismic anisotropy
Okavango rift zone
shear wave splitting

ABSTRACT

This study represents the first shear-wave splitting investigation of the Okavango rift zone (ORZ), an incipient continental rift belonging to the East African rift system in northern Botswana. Analysis of broadband seismic data recorded along a 750 km long profile of 22 stations traversing the ORZ and adjacent Congo and Kalahari cratons and several Precambrian orogenic zones reveals dominantly NE–SW fast orientations, which are parallel to both the absolute plate motion direction (based on the NNR-NUVEL-1A model) and the trend of most tectonic boundaries, including that of the ORZ. Spatial coherence analysis of the splitting parameters and correspondence between the observed fast orientations and the trend of tectonic features indicate that the main source of observed anisotropy is most likely in the upper asthenosphere, probably due to simple shear associated with the relative movement of the lithosphere against the asthenosphere. The presence of consistently rift-parallel fast orientations and normal splitting times in the ORZ and most parts of southern Africa implies that neither an upper mantle plume nor small-scale convection is the dominant source for rift initiation and development. The first shear-wave splitting measurements in the vicinity of the ORZ favor a model in which continental rifting develops in response to intra-plate relative movement of continental blocks along zones of weakness produced by ancient tectonic events.



## 1. Introduction

Continental rifting constitutes the transition from stable continental lithosphere into an ocean basin. Numerous studies suggested that continental rifting is either induced by active mantle upwelling associated with deep mantle plumes (active rifting), or by horizontal motion of plates and their interaction along plate boundaries (passive rifting; Sengor and Burke, 1978; Hill, 1991). These contrasting models of continental rupture are primarily assembled from observations of mature rift zones. In contrast, knowledge of rifting mechanisms and the associated characteristic lithospheric and asthenospheric structure and dynamics beneath incipient rift zones, such as the Okavango rift zone (ORZ) in northern Botswana, is severely limited.

The ORZ (Fig. 1) is one of the youngest continental rifts in the world with an estimated initiation of surface rupture between 120 and 40 ka (Kinabo et al., 2008) and thus is an ideal locale to study the characteristics of earliest-stage rifting mechanisms. Situated at the southwestern terminal of the East African rift system (EARS), the ORZ is superimposed upon the Neoproterozoic Damara belt and Paleoproterozoic Rehoboth province (McCourt et al., 2013), which are bounded toward the northwest and southeast by the Congo and Kalahari cratons, respectively (Begg et al., 2009). The latter is a composite terrane composed largely of the Archean Kaapvaal and Zimbabwe cratons and the Archean Limpopo belt. It is encircled by the Paleo- to Mesoproterozoic Namaqua-Natal belt to the south and the Paleoproterozoic Magondi belt and Rehoboth province toward the west (McCourt et al., 2013) (Fig. 1).

While the crustal and mantle structure and dynamics of the Kalahari craton and the mature sections of the EARS have been extensively studied through numerous projects over the past 40 years, the ORZ has not been investigated using robust structural seismological techniques. One such technique is shear-wave splitting (SWS) analysis. It has long been recognized that near-vertically incident shear waves propagating in a transversely isotropic medium split into two waves with orthogonal polarization orientations (Crampin, 1981). SWS analysis is commonly employed to quantify in-situ lithospheric and asthenospheric seismic anisotropy (e.g., Silver and Chan, 1991). It uses P-to-S converted phases at the core–mantle boundary, including PKS, SKKS, and SKS (which are collectively called XKS), to obtain the two split-

* Corresponding author.
*E-mail address:* liukh@mst.edu (K.H. Liu).

http://dx.doi.org/10.1016/j.epsl.2015.08.009
0012-821X/

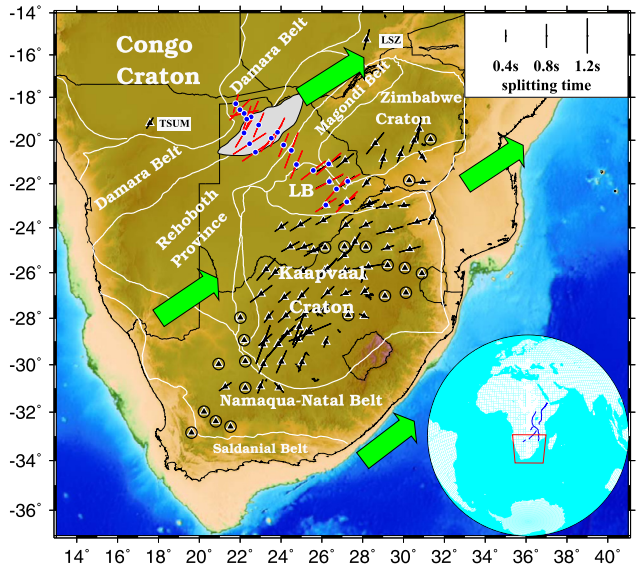


**Fig. 1.** A topographic map of southern Africa showing the major tectonic provinces and station-averaged shear-wave splitting measurements from this (blue dots and red bars) and previous (black triangles and bars) studies (Vinnik et al., 1996; Barruol and Ismail, 2001; Silver et al., 2001). Black circles represent null measurements. The Okavango rift zone is highlighted by the grey infilled area. Green arrows represent the APM direction based on the NUVEL-1A model (DeMets et al., 1994). Major tectonic boundaries are plotted as white lines modified from McCourt et al. (2013). LB: Limpopo belt. Note that the Kaapvaal and Zimbabwe cratons and the Limpopo belt are components of the Kalahari craton. The inset shows the location of southern Africa indicated by the red rectangle and the blue lines represent the rift axes of the East African rift system. (For interpretation of the references to color in this figure legend, the reader is referred to the web version of this article.)

ting parameters, including the polarization orientation of the fast component (fast orientation or $\phi$), and the splitting time between the fast and slow components (splitting time or $\delta t$). The former is an indicator of the orientation of the anisotropic structure, and the latter measures the strength of anisotropy integrated over the whole raypath from the core–mantle boundary to the recording station.

Seismological and petrophysical studies (e.g., Silver, 1996; Debayle and Ricard, 2013) have indicated that the dominant contribution to splitting parameters lies primarily within the upper mantle. Several mechanisms have been postulated to produce observed tectonic-scale observable anisotropy. Based upon the strong correlation between splitting parameters and surficial geologic features, seismic anisotropy has been proposed to exist in the lithosphere due to fabrics generated by vertically-coherent lithospheric deformation (Silver, 1996; Silver et al., 2001), or lithosphere-scale magmatic dikes (Gao et al., 1997). Alternatively, seismic anisotropy may be induced by present-day upper-mantle flow either as a consequence of simple shear between the rigid lithosphere and mobile asthenosphere, which in turn would produce anisotropy parallel to the absolute plate motion (APM), if the direction of the shear is the same as the APM direction (e.g., Vinnik et al., 1996; Barruol and Ismail, 2001; Gao et al., 2010; Lemnifi et al., 2015), or by small-scale mantle convection (e.g., Gao et al., 1994; Koch et al., 2012). A recent global-scale surface wave azimuthal anisotropy study (Debayle and Ricard, 2013) suggested a weak correlation between APM and fast orientations for plates moving at a rate slower than 2.5 cm/yr; such a correlation increases rapidly for plates moving between 2.5 and 5.5 cm/yr, and saturates for those moving faster than 5.5 cm/yr (see Fig. 6 of Debayle and Ricard, 2013). Note that according to the no-net rotation (NNR) NUVEL-1A model (DeMets et al., 1994), the African continent moves at a rate of 2.8–3.2 cm/yr toward the northeast, and thus the APM is expected to be marginally correlated with the fast orientations if the relationship revealed by Debayle and Ricard (2013) applies precisely for Africa.

SWS studies have been widely conducted in numerous regions of continental rifting affinities. Consistently rift-parallel fast orientations and splitting times substantially larger than the global average of 1.0 s (Silver, 1996) were obtained for the Afar and Main Ethiopian (Gashawbeza et al., 2004; Kendall et al., 2006; Gao et al., 2010), eastern African (Bagley and Nyblade, 2013), Rio Grande (Sandvol et al., 1992; Liu et al., 2014; Refayee et al., 2014), and Baikal (Gao et al., 1997) rifts. Such rift-parallel anisotropy has been attributed to a number of mechanisms, including rift-parallel mantle flow (Sandvol et al., 1992; Gao et al., 2010; Bagley and Nyblade, 2013), lithospheric fabrics formed by past tectonic events (Gashawbeza et al., 2004), and rift-parallel lithospheric dikes (Gao et al., 1997). Rift-orthogonal anisotropy observed in the flanking area of the Baikal rift was hypothesized as reflecting the horizontal branches of a small-scale mantle convection system (Gao et al., 1994, 1997).

In general, most modern continental rift zones are associated with rift-parallel fast orientations. Major exceptions to this observation include the Baikal rift zone and the Red Sea which has partially transitioned into an oceanic spreading center. Recent SWS studies (Elsheikh et al., 2014; Lemnifi et al., 2015) in northern Africa and Arabia revealed N–S fast orientations on both sides of the Red Sea, which has a nearly NW–SE strike. Such N–S orientated anisotropy observed in northern Africa and Arabia was proposed to be the result of simple shear developed in the boundary layer between the lithosphere and the asthenosphere formed by long-term northward motion of the African plate relative to the asthenosphere (Elsheikh et al., 2014; Lemnifi et al., 2015).

Splitting measurements are absent in the vicinity of the ORZ due to the heretofore paucity of broadband seismic data. Previous measurements in southern Africa were concentrated on the Kaapvaal and Zimbabwe cratons and the Limpopo belt (Fig. 1). An investigation by Vinnik et al. (1996) at 7 stations on the Kaapvaal craton revealed NE–SW oriented fast orientations, which are parallel to the APM direction of Africa since the Jurassic computed based on the NNR-NUVEL-1A model (DeMets et al., 1994), and were therefore interpreted to be the result of APM induced asthenospheric flow. Subsequently, Silver et al. (2001) used a much larger data set recorded at 79 sites in southern Africa and proposed that the observed anisotropy is the result of vertically-coherent lithospheric deformation. Surface-wave studies beneath southern Africa suggested that azimuthal anisotropy varies with depth, implying the presence of anisotropy both in the lithosphere and asthenosphere (Adam and Lebedev, 2012).

This study is part of a multi-disciplinary investigation of the incipient segments of the EARS (Gao et al., 2013). Our main objective is to present results from the first examination of mantle anisotropy using SWS in the vicinity of the ORZ in order to provide constraints on models of rift initiation and anisotropy formation. In doing so, we explore possible relationships between the observed anisotropy with predicted directions of rifting-related mantle flow, the direction of present-day plate motion, and the dominant trend of Precambrian tectonic boundaries.

## 2. Data and methods

### 2.1. Data

The broadband seismic data used in the study were recorded by 17 Seismic Arrays for African Rift Initiation (SAFARI) stations that we installed and operated for a two-year period starting from the summer of 2012 (Gao et al., 2013). Data recorded by five stations belonging to the 1997–99 Southern African Seismic Experiment (SASE; Silver et al., 2001) situated immediately within our study

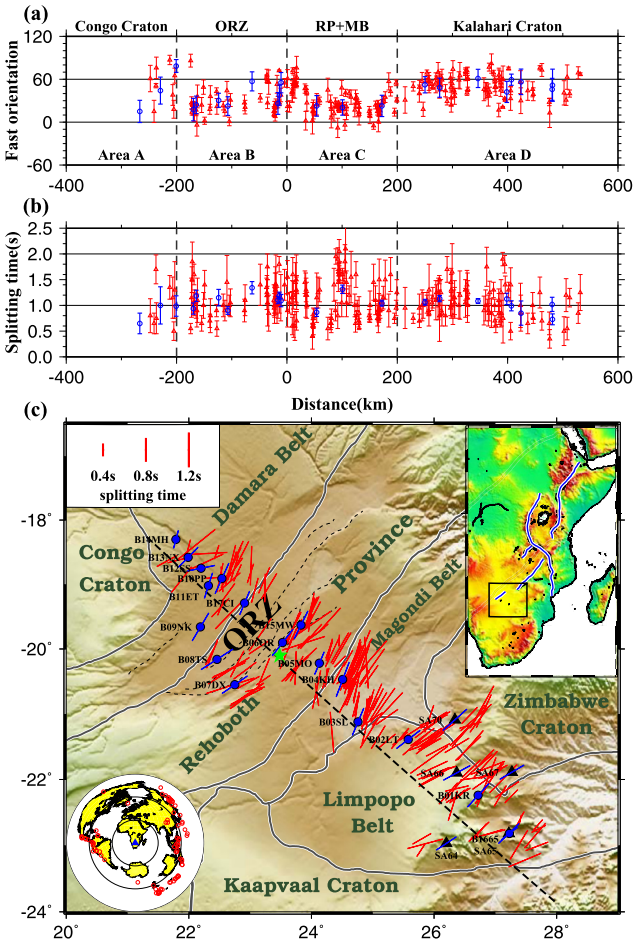


**Fig. 2.** Cross-section and map views of the resulting splitting parameters. (a) Fast orientations projected to the thick dashed profile in (c). Blue bars represent the station-averaged values of the fast orientation while the red bars indicate each individual measurement. RP: Rehoboth province; MB: Magondi belt. (b) Same as (a) but for splitting times. (c) Individual splitting parameters (red) plotted at the 250 km depth ray-piercing points, and station-averaged parameters (blue) plotted at the location of the stations. Grey lines delineate the tectonic provinces, and thin dashed lines within the ORZ area show active faults (Kinabo et al., 2008). SAFARI stations are shown as blue dots and SASE ones as black triangles. The inset in the upper-right corner displays the location of the study area while the one in the lower-left corner shows the distribution of earthquakes (red circles) used in the study. The green star near the SE border of the ORZ marks origin point (zero distance) in (a) and (b). (For interpretation of the references to color in this figure legend, the reader is referred to the web version of this article.)

area are also used. One of the SAFARI stations, B1665, is located about 1 km away from SASE station SA65 (Fig. 2). The total length of the profile is about 750 km (Figs. 1 and 2). XKS waveforms were requested from the Incorporated Research Institutions for Seismology (IRIS) Data Management Center (DMC). The epicentral distance range for PKS, SKKS, and SKS is 120–180°, 95–180° and 84–180°, respectively (Liu and Gao, 2013). We apply a cutoff magnitude of 5.6 for events shallower than 100 km while allow for magnitudes from deeper events as low as 5.5 for the purpose of taking advantage of sharper waveforms.

To identify and correct for possible sensor misorientation, we apply the technique developed by Niu and Li (2011) to minimize the P-wave energy on the transverse component. We begin by manually picking the first arrival of the direct P-phase on the vertical component for events recorded by no fewer than 5 stations. The optimal orientation of the N–S component corresponding to the minimum P-wave energy on the transverse component is found using a grid-search algorithm, and is subsequently used to correct for station orientation prior to SWS analysis.

### 2.2. Measuring shear-wave splitting parameters

SWS parameters were calculated using the procedure of Liu and Gao (2013) which was based on the method of minimization of transverse energy (Silver and Chan, 1991). The seismograms were first windowed to include the theoretical arrival of the individual XKS phases and then enhanced by applying a band-pass filter with corner frequencies of 0.04–0.5 Hz. All the SWS measurements were visually verified and, if necessary, various adjustments were applied to the beginning and end times of the XKS window, quality ranking, and/or band-pass filtering frequencies to ensure reliability (Liu and Gao, 2013).

Following the evaluation criteria of Liu and Gao (2013), we ranked well-defined splitting measurements as either A (outstanding) or B (good) for use in the following SWS analyses. We also analyzed the data set for null measurements, which are characterized by a lack of observable energy on the transverse component concurrent with a strong XKS arrival on the radial component. Situations wherein the backazimuth (BAZ) is parallel or perpendicular to the fast orientation, or the sub-station crust and mantle are isotropic, can all result in null measurements (Silver and Chan, 1991; Liu and Gao, 2013). As shown in Fig. 2, well-defined splitting parameters were observed at all stations in the study area, suggesting the existence of pervasive anisotropy. Consequently, null measurements will not be discussed below.

### 2.3. Anisotropy depth determination

The epicentral distance of the SKS, SKKS, and PKS arrivals used in the study is equal to or greater than 84°, 95°, and 120°, respectively. For SKS, this corresponds to a ray parameter of 6.532 s/degree or smaller, and an angle of incidence of smaller than 16° at 200 km depth measured from the vertical. Similarly, the maximum angle of incidence at 200 km depth for the SKKS and PKS phases is about 18° and 5°, respectively. Therefore, the XKS phases arrive at a steep angle of incidence and thus have an excellent lateral but poor vertical resolution, resulting in uncertainties and debates in the tectonic interpretations of the observed SWS measurements.

A technique commonly employed to estimate anisotropy depth is the intersecting Fresnel-zone approach (Alsina and Snieder, 1995) which is based on the analysis of the size for the first Fresnel zones of close-proximity XKS raypaths. However, such a technique is limited to the case wherein significant lateral variations in seismic anisotropy exist between nearby stations, or when a station samples two regions with different splitting parameters (see Lemnifi et al., 2015 for an example in Libya).

In this study, we apply a more generalized and quantitative extension of the intersecting Fresnel zone approach based on the spatial coherency of splitting parameters (Liu and Gao, 2011). This technique employs the idea that the observed splitting parameters will reach the highest spatial coherency if the assumed anisotropy depth is correct.

The optimal anisotropy depth is searched in the range of 0 to 350 km at an interval of 5 km. It corresponds to the minimum spatial variation factor ($F_v$), which is defined in Eqs. (4)–(7) in Liu and Gao (2011). The block size ($dx$) used to calculate the $F_v$ should be given a proper value due to the fact that smaller $dx$ will bring unstable $F_v$ depth variations and uncertainties, while larger $dx$ leads to a broadened $F_v$ curve and reduces the peak-to-peak amplitude (Liu and Gao, 2011). In this study, experimental values of $dx$ from 0.16° to 0.28° with an interval of 0.02° have been employed to generate the $F_v$ curves.

**Table 1**
Resulting orientation of the N–S component.

| Station | | | AZ (deg.) | No. events |
|---|---|---|---|---|
| Name | Lat. (deg.) | Lon. (deg.) | | |
| B01KR | −22.238 | 26.718 | −1 | 102 |
| B02LT | −21.393 | 25.581 | 2 | 125 |
| B03SL | −21.121 | 24.764 | −6 | 135 |
| B04KH | −20.474 | 24.514 | −2 | 125 |
| B05MO | −20.218 | 24.132 | −6 | 131 |
| B06OR | −19.901 | 23.527 | −10 | 155 |
| B07DX | −20.549 | 22.749 | −11 | 115 |
| B08TS | −20.164 | 22.459 | 0 | 84 |
| B09NK | −19.663 | 22.194 | −16 | 114 |
| B10PP | −18.913 | 22.543 | 5 | 118 |
| B11ET | −19.016 | 22.316 | −1 | 112 |
| B12SS | −18.746 | 22.197 | 3 | 108 |
| B13NX | −18.579 | 21.994 | 4 | 100 |
| B14MH | −18.295 | 21.792 | −4 | 117 |
| B15MW | −19.631 | 23.827 | −9 | 97 |
| B1665 | −22.825 | 27.229 | −4 | 130 |
| B17CI | −19.294 | 22.909 | −13 | 50 |
| SA64 | −22.969 | 26.202 | 3 | 34 |
| SA65 | −22.818 | 27.222 | 2 | 39 |
| SA66 | −21.900 | 26.373 | −3 | 38 |
| SA67 | −21.886 | 27.274 | −1 | 35 |
| SA70 | −21.088 | 26.335 | −4 | 41 |

## 3. Results

### 3.1. Sensor orientation correction

Table 1 shows the optimal orientation of the N–S component of the 3-component sensor for each of the 22 stations. The magnitude of the orientation ranges from −16 to 5° clockwise from the north, with a simple mean of $-3 \pm 1°$. The overwhelmingly negative values of the resulting orientation were most likely the consequences of inadequate correction of the declination of the geomagnetic field, which is about −9° in the study area.

After the application of station orientation correction, the quality of the resulting SWS measurements at stations with misoriented sensors is noticeably improved. Fig. 3 shows an example of the improvement for station B07DX. When the uncorrected data are used for SWS analysis, remaining XKS energy on the corrected transverse seismogram is observable, and the match between the fast and slow components is poor and is accompanied by weak linearity of the corrected particle motion (Fig. 3A). All of these features are indicators of sensor misorientation, as discussed in Liu et al. (2008). The post orientation correction measurement is substantially improved in terms of the removal of transverse energy, the matching of the fast and slow waveforms, and the linearity of the particle motions (Fig. 3B).

### 3.2. Spatial distribution of XKS splitting parameters

A total of 223 pairs of Quality A or B splitting parameters were obtained at the 22 stations, including 73 PKS, 58 SKKS, and 92 SKS measurements from a total of 91 teleseismic events (Fig. 2c). Examples for each of the three XKS phases are demonstrated in Fig. 4. No systematic azimuthal variations of the splitting parameters are observed (Fig. 5), suggesting that a single layer of anisotropy with a horizontal axis of symmetry is sufficient to explain the observed SWS parameters (Silver and Savage, 1994). The fast orientations are dominantly NE–SW with an average value of $37.5 \pm 20.6°$ (Figs. 1 and 2, Table 2), which is consistent with the APM direction of the African plate in the study area based on the NNR-NUVEL-1A model (DeMets et al., 1994). The mean splitting time is $1.09 \pm 0.34$ s and is comparable with the global average of 1.0 s for continents (Silver, 1996), but is larger than the 0.62

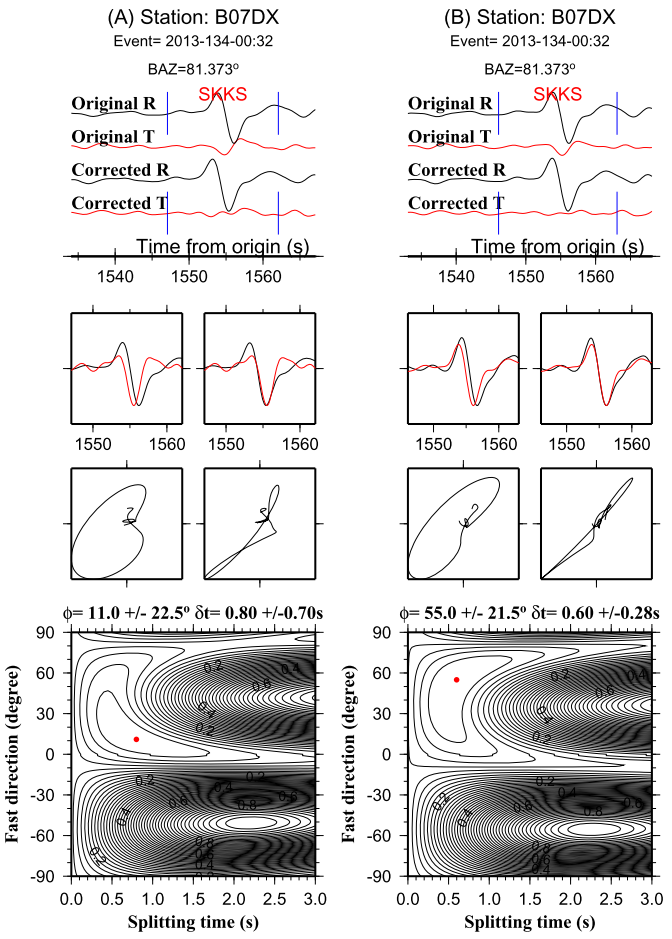


**Fig. 3.** An SKKS measurement from station B07DX (at which the N–S component has an orientation of −11°) calculated using (A) the original and (B) station-orientation corrected dataset, respectively. (Top) Original and corrected XKS radial and transverse component seismograms. (Middle) Pre- and post-correction fast and slow waveforms and particle motion patterns. (Bottom) Contour maps of transverse component energy. The red dot on the contour map indicates the optimal splitting parameters. (For interpretation of the references to color in this figure legend, the reader is referred to the web version of this article.)

**Table 2**
Station-averaged splitting parameters.

| Station | | | $\phi$ (deg.) | $\delta t$ (s) | No. events |
|---|---|---|---|---|---|
| Name | Lat. (deg.) | Lon. (deg.) | | | |
| B01KR | −22.238 | 26.718 | 42 ± 14 | 1.13 ± 0.43 | 15 |
| B02LT | −21.393 | 25.581 | 52 ± 11 | 1.06 ± 0.24 | 19 |
| B03SL | −21.121 | 24.764 | 22 ± 14 | 1.04 ± 0.27 | 21 |
| B04KH | −20.474 | 24.514 | 20 ± 10 | 1.31 ± 0.45 | 31 |
| B05MO | −20.218 | 24.132 | 22 ± 14 | 0.87 ± 0.32 | 16 |
| B06OR | −19.901 | 23.527 | 37 ± 14 | 1.19 ± 0.26 | 15 |
| B07DX | −20.549 | 22.749 | 55 ± 14 | 1.09 ± 0.34 | 8 |
| B08TS | −20.164 | 22.459 | 57 ± 13 | 1.34 ± 0.32 | 7 |
| B09NK | −19.663 | 22.194 | 30 ± 9 | 1.15 ± 0.28 | 3 |
| B10PP | −18.913 | 22.543 | 24 ± 12 | 1.19 ± 0.36 | 11 |
| B11ET | −19.016 | 22.316 | 17 ± 15 | 0.94 ± 0.22 | 4 |
| B12SS | −18.746 | 22.197 | 78 ± 8 | 0.99 ± 0.40 | 4 |
| B13NX | −18.579 | 21.994 | 44 ± 18 | 1.00 ± 0.63 | 3 |
| B14MH | −18.295 | 21.792 | 15 ± 15 | 0.65 ± 0.20 | 1 |
| B15MW | −19.631 | 23.827 | 26 ± 15 | 1.11 ± 0.24 | 11 |
| B1665 | −22.825 | 27.229 | 51 ± 22 | 0.73 ± 0.28 | 7 |
| B17CI | −19.294 | 22.909 | 22 ± 13 | 0.90 ± 0.18 | 6 |
| SA64 | −22.969 | 26.202 | 56 ± 17 | 0.85 ± 0.41 | 3 |
| SA65 | −22.818 | 27.222 | 45 ± 15 | 1.02 ± 0.31 | 5 |
| SA66 | −21.900 | 26.373 | 61 ± 12 | 1.09 ± 0.15 | 10 |
| SA67 | −21.886 | 27.274 | 59 ± 7 | 0.99 ± 0.24 | 6 |
| SA70 | −21.088 | 26.335 | 48 ± 13 | 1.13 ± 0.25 | 17 |

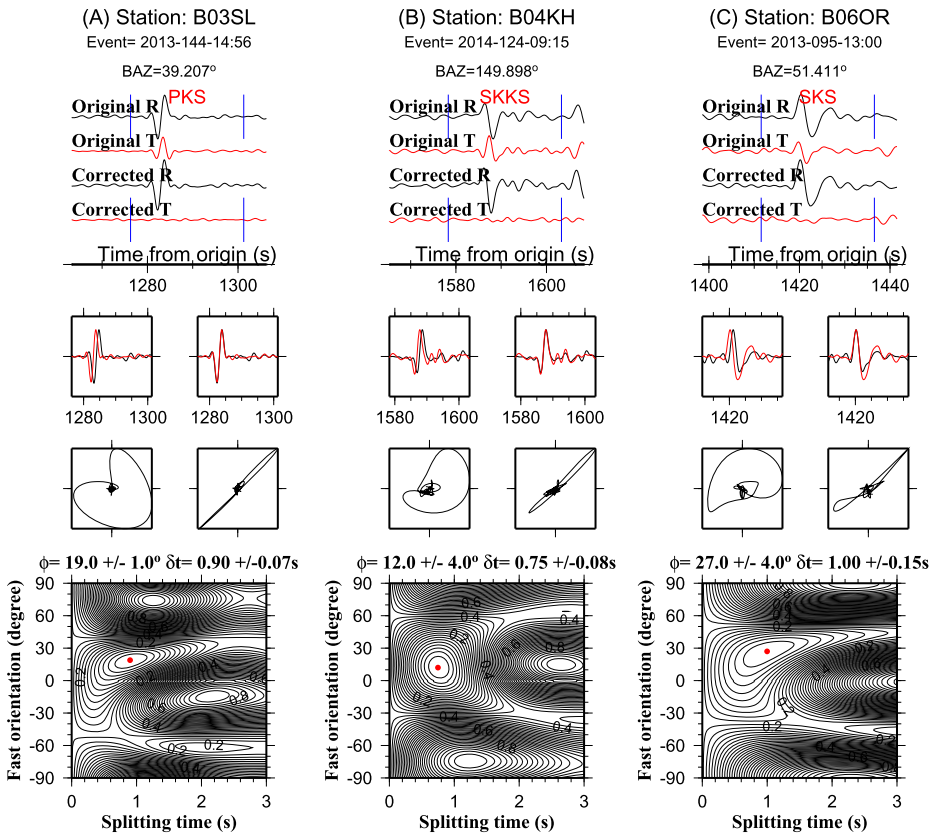


**Fig. 4.** Same as Fig. 3 but for examples of each of the XKS phases (PKS, SKKS and SKS) used in the study recorded by 3 different stations. The waveforms have been corrected for station mis-orientation.

± 0.02 s observed at the 59 non-null SASE stations (Silver et al., 2001). Under the assumption of a 4% anisotropy (Mainprice et al., 2000), the thickness of the anisotropy layer that produces the observed anisotropy is about 120 km on average.

Based on the location of the tectonic boundaries (Begg et al., 2009; McCourt et al., 2013) and the characteristics of the observed splitting parameters, we divide the measurements into 4 groups (Fig. 2a). The 7 measurements in Area A (Figs. 5a and 5b) have the surface projection of their ray-piercing points (calculated at the depth of 250 km) on the Congo craton. The mean splitting parameters are 56.1 ± 24.1° for $\phi$, and 1.10 ± 0.38 s for $\delta t$. The 48 Area B measurements are in the ORZ, with corresponding mean splitting parameters of 30.3 ± 19.3° and 1.12 ± 0.31 s (Figs. 5c and 5d). Area C includes 83 measurements in the Magondi belt and the southern half of the Rehoboth province (Figs. 5e and 5f). The mean splitting parameters are 27.3 ± 17.4° and 1.13 ± 0.40 s. The most significant spatial variation of the splitting parameters in the entire study is found near the SE end of Area C (Fig. 2a). Area D belongs to the Kalahari craton (mostly the Limpopo belt). It has 85 measurements (Figs. 5g and 5h) and the mean splitting parameters are 50.16 ± 15.7° and 1.04 ± 0.30 s.

### 3.3. Relationship with SWS studies from adjacent areas

All of the previous studies in adjacent areas reported their results in the form of station-averaged parameters, which are largely consistent with those obtained at 22 stations measured by this study (Fig. 1). Barruol and Ismail (2001) used African IRIS and Geoscope permanent stations to investigate upper mantle anisotropy, including station TSUM in Namibia near the southern border of the Congo craton as well as station LSZ in Zambia northeast of the ORZ (Fig. 1). Both LSZ and TSUM display SWS parameters consistent with our findings, i.e., a nearly NE–SW fast orientation (16° and 31°, respectively) and small splitting time (0.73 s and 0.43 s, respectively) without evidence of azimuthal variations. Similarly, relatively small splitting times are observed for the SAFARI stations near the Congo craton (e.g., B14MH and B13NX) while relatively larger splitting times are reported for stations within the ORZ (about 1.12 s on average).

Among the 17 SAFARI stations, three (B01KR, B02LT, and B1665) are within the study area of the SASE project (Silver et al., 2001). The resulting SWS parameters from the three SAFARI stations are remarkably consistent with those from the five SASE stations along the profile (Silver et al., 2001). The average fast orientation and splitting time of the five SASE stations are 53.4 ± 14.6° and 1.07 ± 0.25 s, while those of the three SAFARI stations are 48.2 ± 15.7° and 1.03 ± 0.35 s. The individual SWS measurements demonstrating an approximate E–W fast orientation are similar with the station-averaged SWS measurements obtained by Silver et al. (2001) from other SASE stations within the Limpopo belt (Figs. 1 and 2).

## 4. Discussion

### 4.1. Depth of anisotropy

Several conditions must be satisfied prior to applying the anisotropy-depth estimation technique (Liu and Gao, 2011), the first of which is the compilation of a high-quality data set of individual (rather than station-averaged) splitting parameters, and the other is that there must exist a significant but smooth spatial variation in the splitting parameters which should simultaneously signify a single layer of anisotropy (Liu and Gao, 2011). We find that the observed SWS measurements in Area C possess significant spatial variations (Fig. 2a) and satisfy the other conditions mentioned above, and can be used to estimate the depth of anisotropy.

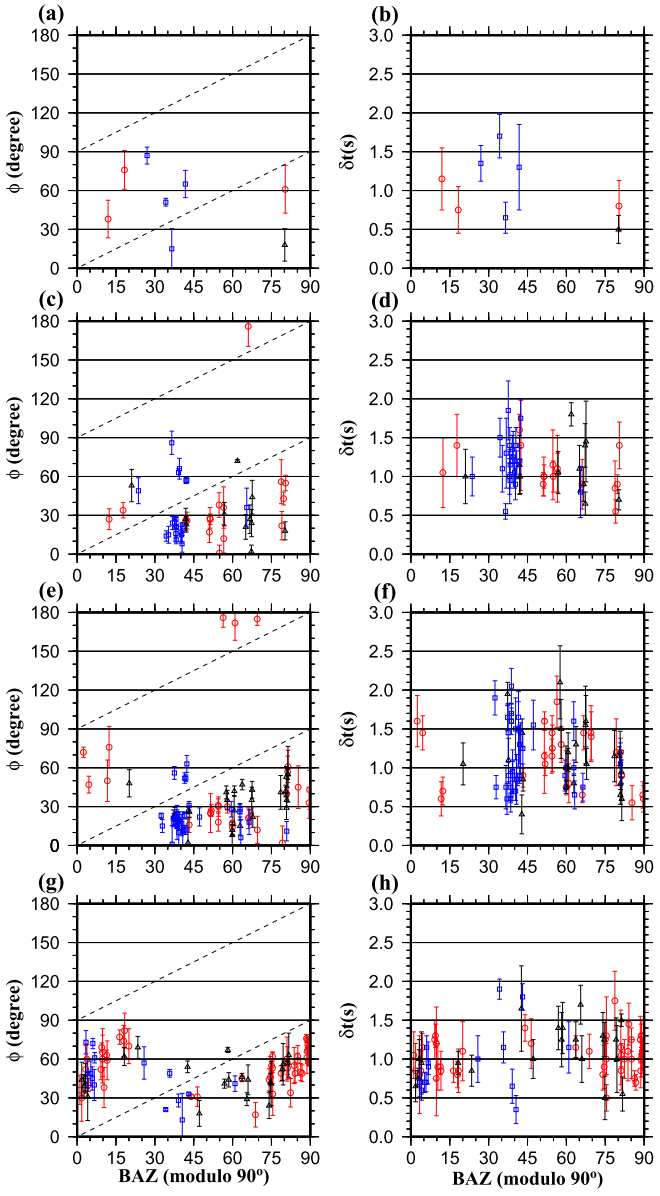


**Fig. 5.** Azimuthal variations of resulting fast orientations (left panels) and splitting times (right panels) for (a, b) Area A, (c, d) Area B, (e, f) Area C, and (g, h) Area D measurements. Blue squares, black triangles, and red circles represent PKS, SKKS, and SKS phases, respectively. The dashed lines show the situation when the BAZ equals $\phi$ or $\phi + 90°$, i.e., along the lines null measurements are expected (and this is why there are no well-defined measurements along the lines). (For interpretation of the references to color in this figure legend, the reader is referred to the web version of this article.)

The depths corresponding to the minimum variation factor on the resulting $F_v$ curves (Fig. 6) calculated using the spatial coherency technique suggest that the optimal depth of the center of the anisotropic layer is approximately between 240 and 280 km, which is similar to the lithospheric thickness based on the tomography results for southern Africa (James et al., 2001). Beneath the vicinity of the ORZ, magnetotelluric studies suggested a lithospheric thickness of about 180 km (Miensopust et al., 2011), and surface wave tomography revealed a similar thickness of 180–220 km (Fishwick, 2010). Thus it can be safely concluded that the anisotropy originates primarily from the upper asthenosphere beneath the ORZ, which is similar to the conclusion proposed by Vinnik et al. (1996) for the Kaapvaal craton. It must be mentioned that due to a lack of spatial variations of the splitting parameters in Areas A, B, and D, the depth of the source of

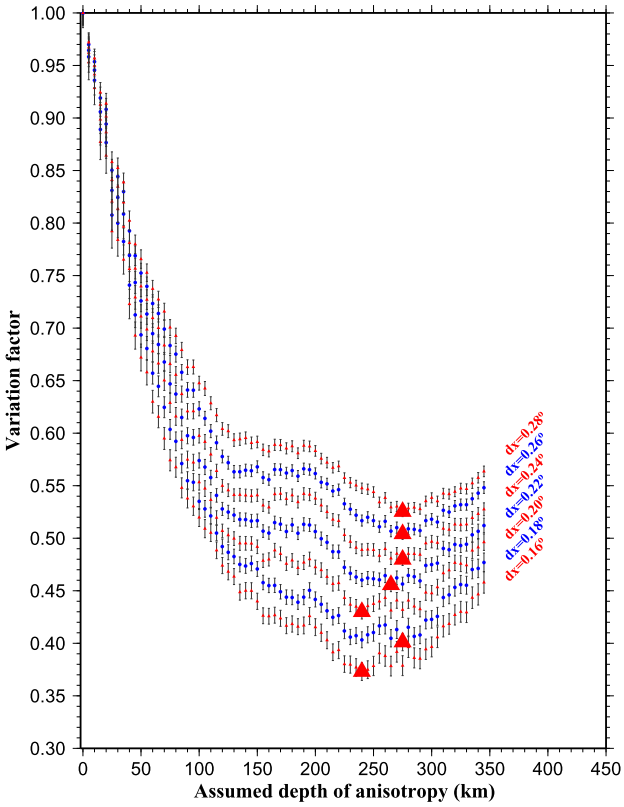


**Fig. 6.** Anisotropy analysis for the SWS measurements in Area C based on the spatial coherence technique (Liu and Gao, 2011), resulting in an optimal depth of anisotropy between 240 and 280 km. The triangle on each of the curves marks the depth with the minimum variation factor.

the observed anisotropy cannot be estimated beneath these areas; however, as discussed below, although lithospheric contributions cannot be completely ruled out, the observations can best be explained if they have an asthenospheric origin.

### 4.2. Constraints on rifting mechanisms

The similarity between the APM direction and the trend of most of the tectonic boundaries in the study area makes it difficult to distinguish a lithospheric origin from an asthenospheric one. In addition to the results of depth estimation, which favors an upper asthenospheric origin, another piece of evidence arguing against a dominantly lithospheric origin can be found along the boundary between the Zimbabwe craton and the Limpopo belt (Fig. 2), where all the fast orientations are almost orthogonal (rather than parallel, as expected for a lithospheric origin) to this major tectonic boundary. Additionally, the ORZ, which is characterized by a relatively thin lithosphere compared to the adjacent cratonic terranes based upon magnetotelluric and tomographic studies (James et al., 2001; Miensopust et al., 2011), exhibits slightly larger splitting times than the Kalahari craton. One would expect to observe smaller splitting times in regions with thin lithosphere if the anisotropy is the result of uniform strain pervading the continental lithosphere (Silver and Chan, 1991). This interpretation is also consistent with the fact that the SASE stations (Silver et al., 2001), most of which overlie the thicker lithosphere of the Kalahari craton, show smaller splitting times with a mean value of 0.62 ± 0.02 s (and about 1/4 of the stations show no splitting) relative to the SAFARI stations (1.09 ± 0.34 s).

In the following, we examine a number of possible geodynamic models for the initiation and development of continental rifting, under the assumption that the observed anisotropy primarily re-

flects simple shear in an approximately 120 km thick layer in the upper-most asthenosphere.

#### 4.2.1. Active rifting

Active rifting models (e.g., Sengor and Burke, 1978) advocate the dominant role of mantle flow, presumably associated with a mantle plume, on continental breakup. For a stationary lithosphere relative to the asthenosphere, the horizontal component of the flow system is expected to have a pattern that is radiating away from the center of the plume, and for a moving lithosphere, a parabolic pattern is predicted (Karato et al., 2008).

The existence of such a plume beneath the ORZ is possible, due to the fact that the ORZ is developing directly above the proposed African superplume (Ritsema et al., 1998; Hansen et al., 2012). The expected radiating or parabolic pattern of the fast orientations, however, is not observed beneath the ORZ or in southern Africa (Fig. 1), leading to doubts about the existence of an active mantle plume beneath the area. Such a conclusion is consistent with the observations of normal mantle transition zone thickness using the same dataset (Yu et al., 2015), as well as results from seismic tomography studies suggesting that the Superplume beneath southern Africa is limited in the lower mantle (e.g., Ritsema et al., 1998).

#### 4.2.2. Edge-driven mantle convection

The thin lithosphere beneath the ORZ relative to the Congo craton could induce a small-scale mantle convection system due to lateral temperature variations (King and Anderson, 1998). This mechanism has been used to explain the formation of zones of continental extension such as the Cameroon volcanic line (Koch et al., 2012), although other mechanisms such as three-dimensional convective instability at the base of the lithosphere (Fourel et al., 2013) have been proposed to explain volcanisms along the edge of the Congo craton. If this process contributes significantly to the observed anisotropy, the fast orientations in the vicinity of the ORZ should be mostly orthogonal to the trend of the rift. We observed dominantly rift-parallel fast orientations and thus conclude that edge-driven small-scale convection is not the source of the observed anisotropy.

#### 4.2.3. Rifting induced by intra-plate relative motion

The ORZ is developing primarily within the Damara orogenic belt between the Archean Congo and Kalahari cratons. The consistently NE–SW fast orientations are largely in agreement with those observed in surrounding areas. Though the African plate has a general northeastward motion based on the NUVEL-1A model (DeMets et al., 1994), it has been suggested that South Africa is currently rotating clockwise relative to the Nubian plate, probably along the Damara belt (Malservisi et al., 2013).

Numerical modeling shows that topography of the lithosphere–asthenosphere boundary exerts a strong control on the direction and magnitude of stress transfer from the asthenosphere to the lithosphere (O'Neill et al., 2010). In addition, increased plate-mantle coupling beneath thick continental lithosphere may increase plate-driving forces, surface deformation, and mantle-derived lithospheric stresses in these regions (Conrad and Lithgow-Bertelloni, 2006). Therefore, contrasts in lithospheric thickness between the Congo craton, the ancient orogenic belts, and the Kalahari craton can possibly lead to differential basal drag forces beneath different areas, leading to spatially-varying plate motion velocities. The relative movements between the Archean cratons could rupture ancient zones of lithospheric weakness such as the Damara belt and exert a trans-tensional force upon the lithosphere, resulting in the initiation of continental rifting. This is consistent with the observation that most rifts develop within weak orogenic zones (Keller et al., 1991; Vauchez et al., 1997). The spatially consistent NE–SW fast orientations observed in the study area as well as the rest of southern Africa are mostly parallel to the APM predicted by the NUVEL-1A model, which suggests a plate motion rate of about 3 cm/yr. This is slightly above the threshold value of 2.5 cm/yr (Debayle and Ricard, 2013), above which a moving plate is expected to exert simple shear to the asthenosphere and induce azimuthal anisotropy.

This model suggests a passive role of mantle flow in the initiation and development of the ORZ. Given the consistency between the APM and the fast orientations revealed by this and previous studies (Fig. 1), we propose that simple shear in the direction of the APM developed in the upper asthenosphere contributes the bulk of the observed anisotropy. Deviations of the fast orientation observed in Area C can be explained as the modulation of flow by the topography of the bottom of the lithosphere, as proposed for North America (Fouch et al., 2000; Refayee et al., 2014) and northern Africa (Lemnifi et al., 2015). The model is consistent with surface wave studies which demonstrate the existence of asthenospheric plate-parallel polarization of azimuthal anisotropy beneath southern Africa (Adam and Lebedev, 2012), and with findings from a joint inversion of P-wave receiver functions and SWS waveforms (Vinnik et al., 2012).

## 5. Conclusions

In this study, we employed recently recorded broadband seismic data in the vicinity of the ORZ to conduct the first SWS investigation of the incipient rift. The resulting mantle anisotropy shows a dominantly NE–SW orientation which is parallel to the African APM. Although significant contributions from the lithosphere to the observed anisotropy cannot be completely ruled out, spatial coherency analysis of the splitting parameters and correspondence with geological features suggest that the center of the approximately 120 km thick anisotropic layer is located between the depth of 240 and 280 km, implying an asthenospheric origin of anisotropy, probably as the result of simple shear in the boundary layer between the lithosphere and the asthenosphere. Comparison of the resulting SWS measurements with predicted mantle flow directions originating from an active mantle plume or edge-driven small-scale mantle convection suggests that neither is operating in the upper mantle beneath the incipient rift. The measurements support the rifting initiation model in which differential basal drag applied to cratonic blocks results in relative intra-plate movements, and leads to rifting along ancient orogenic zones, which are areas of mechanical weakness.

## Acknowledgements

Equipment and logistical support was provided by the Portable Array Seismic Studies of the Continental Lithosphere (PASSCAL) Instrument Center. We thank A.M. Reusch from PASSCAL and K. Kaisara from the University of Botswana for their field assistance. Comments from Editor B. Buffett and two anonymous reviewers significantly improved the manuscript. Y.Y. was partially supported by the China Scholarship Council under award 2011645027. This study was supported by the United States National Science Foundation under grant EAR-1009946 to S.G. and K.L.

## References

Adam, J.M.C., Lebedev, S., 2012. Azimuthal anisotropy beneath southern Africa from very broad-band surface-wave dispersion measurements. Geophys. J. Int. 191, 155–174. http://dx.doi.org/10.1111/j.1365-246X.2012.05583.x.

Alsina, D., Snieder, R., 1995. Small-scale sublithospheric continental mantle deformation: constraints from SKS splitting observations. Geophys. J. Int. 123, 431–448. http://dx.doi.org/10.1111/j.1365-246X.1995.tb06864.x.

Bagley, B., Nyblade, A.A., 2013. Seismic anisotropy in eastern Africa, mantle flow, and the African superplume. Geophys. Res. Lett. 40, 1500–1505. http://dx.doi.org/10.1002/grl.50315.

Barruol, G., Ismail, W.B., 2001. Upper mantle anisotropy beneath the African IRIS and Geoscope stations. Geophys. J. Int. 146, 549–561. http://dx.doi.org/10.1046/j.0956-540x.2001.01481.x.

Begg, G.C., Griffin, W.L., Natapov, L.M., O'Reilly, S.Y., Grand, S.P., O'Neill, C.J., Hronsky, J.M.A., Poudjom Djomani, Y., Swain, C.J., Deen, T., Bowden, P., 2009. The lithospheric architecture of Africa: seismic tomography, mantle petrology, and tectonic evolution. Geosphere 5, 23–50. http://dx.doi.org/10.1130/GES00179.1.

Conrad, C.P., Lithgow-Bertelloni, C., 2006. Influence of continental roots and asthenosphere on plate-mantle coupling. Geophys. Res. Lett. 33, L05312. http://dx.doi.org/10.1029/2005GL025621.

Crampin, S., 1981. A review of wave motion in anisotropic and cracked elastic-media. Wave Motion 3, 343–391. http://dx.doi.org/10.1016/0165-2125(81)90026-3.

Debayle, E., Ricard, Y., 2013. Seismic observations of large-scale deformation at the bottom of fast-moving plates. Earth Planet. Sci. Lett. 376, 165–177. http://dx.doi.org/10.1016/j.epsl.2013.06.025.

DeMets, C., Gordon, R.G., Argus, D.F., Stein, S., 1994. Effect of recent revisions to the geomagnetic reversal time scale on estimates of current plate motions. Geophys. Res. Lett. 21, 2191–2194. http://dx.doi.org/10.1029/94GL02118.

Elsheikh, A.A., Gao, S.S., Liu, K.H., Mohamed, A.A., Yu, Y., Fat-Helbary, R.E., 2014. Seismic anisotropy and subduction-induced mantle fabrics beneath the Arabian and Nubian Plates adjacent to the Red Sea. Geophys. Res. Lett. 41, 2376–2381.

Fishwick, S., 2010. Surface wave tomography: imaging of the lithosphere–asthenosphere boundary beneath central and southern Africa? Lithos 120, 63–73. http://dx.doi.org/10.1016/j.lithos.2010.05.011.

Fouch, M.J., Fischer, K., Parmentier, E.M., Wysession, M.E., Clarke, T.J., 2000. Shear-wave splitting, continental keels, and patterns of mantle flow. J. Geophys. Res. 105, 6255–6275. http://dx.doi.org/10.1029/1999JB900372.

Fourel, L., Milelli, L., Jaupart, C., Limare, A., 2013. Generation of continental rifts, basins, and swells by lithosphere instabilities. J. Geophys. Res. 118, 3080–3100. http://dx.doi.org/10.1002/jgrb.50218.

Gao, S., Davis, P.M., Liu, H., Slack, P.D., Zorin, Y.A., Mordvinova, V.V., Kozhevnikov, V.M., Meyer, R.P., 1994. Seismic anisotropy and mantle flow beneath the Baikal rift zone. Nature 371, 149–151. http://dx.doi.org/10.1038/371149a0.

Gao, S., Davis, P.M., Liu, H., Slack, P.D., Rigor, A.W., Zorin, Y.A., Mordvinova, V.V., Kozhevnikov, V.M., Logatchev, N.A., 1997. SKS splitting beneath continental rift zones. J. Geophys. Res. 102, 22,781–22,797. http://dx.doi.org/10.1029/97JB01858.

Gao, S.S., Liu, K.H., Abdelsalam, M.G., 2010. Seismic anisotropy beneath the Afar Depression and adjacent areas: implications for mantle flow. J. Geophys. Res. 115, B12330. http://dx.doi.org/10.1029/2009JB007141.

Gao, S.S., Liu, K.H., Reed, C.A., Yu, Y., Massinque, B., Mdala, H., Moidaki, M., Mutamina, D., Atekwana, E.A., Ingate, S., Reusch, A.M., 2013. Seismic arrays to study African rift initiation. Eos Trans. AGU 94, 213. http://dx.doi.org/10.1002/2013EO240002.

Gashawbeza, E.M., Klemperer, S.L., Nyblade, A.A., Walker, K.T., Keranen, K.M., 2004. Shear-wave splitting in Ethiopia: Precambrian mantle anisotropy locally modified by Neogene rifting. Geophys. Res. Lett. 31, L18602. http://dx.doi.org/10.1029/2004GL020471.

Hansen, S.E., Nyblade, A.A., Benoit, M.H., 2012. Mantle structure beneath Africa and Arabia from adaptively parameterized P-wave tomography: implications for the origin of Cenozoic Afro-Arabian tectonism. Earth Planet. Sci. Lett. 319, 23–34. http://dx.doi.org/10.1016/j.epsl.2011.12.023.

Hill, R.I., 1991. Starting plumes and continental break-up. Earth Planet. Sci. Lett. 104, 398–416. http://dx.doi.org/10.1016/0012-821X(91)90218-7.

James, D.E., Fouch, M.J., VanDecar, J.C., Van Der Lee, S., 2001. Tectospheric structure beneath southern Africa. Geophys. Res. Lett. 28, 2485–2488. http://dx.doi.org/10.1029/2000GL012578.

Karato, S.I., Jung, H., Katayama, I., Skemer, P., 2008. Geodynamic significance of seismic anisotropy of the upper mantle: new insights from laboratory studies. Annu. Rev. Earth Planet. Sci. 36, 59–95. http://dx.doi.org/10.1146/annurev.earth.36.031207.124120.

Keller, G.R., Khan, M.A., Morgan, P., Wendlandt, R.F., Baldridge, W.S., Olsen, K.H., Prodehl, C., Braile, L.W., 1991. A comparative study of the Rio Grande and Kenya rifts. Tectonophysics 197, 355–371. http://dx.doi.org/10.1016/0040-1951(91)90050-3.

Kendall, J.M., Pilidou, S., Keir, D., Bastow, I.D., Stuart, G.W., Ayele, A., 2006. Mantle upwellings, melt migration, and the rifting of Africa: insights from seismic anisotropy. In: Yirgu, G., Ebinger, C.J., Maguire, P.K.H. (Eds.), The Structure and Evolution of the East African Rift System in the Afar Volcanic Province Within the East African Rift System. In: Geol. Soc. Spec. Publ., vol. 259, pp. 55–72.

Kinabo, B.D., Hogan, J.P., Atekwana, E.A., Abdelsalam, M.G., Modisi, M.P., 2008. Fault growth and propagation during incipient continental rifting: insights from a combined aeromagnetic and Shuttle Radar Topography Mission digital elevation model investigation of the Okavango Rift Zone, northwest Botswana. Tectonics 27, TC3013. http://dx.doi.org/10.1029/2007TC002154.

King, S.D., Anderson, D.L., 1998. Edge-driven convection. Earth Planet. Sci. Lett. 160, 289–296. http://dx.doi.org/10.1016/S0012-821X(98)00089-2.

Koch, F.W., Wiens, D.A., Nyblade, A.A., Shore, P.J., Tibi, R., Ateba, B., Tabod, C.T., Nnange, J.M., 2012. Upper-mantle anisotropy beneath the Cameroon Volcanic Line and Congo craton from shear wave splitting measurements. Geophys. J. Int. 190, 75–86. http://dx.doi.org/10.1111/j.1365-246X.2012.05497.x.

Lemnifi, A.A., Liu, K.H., Gao, S.S., Reed, C.A., Elsheikh, A.A., Yu, Y., Elmelade, A.A., 2015. Azimuthal anisotropy beneath north central Africa from shear wave splitting analyses. Geochem. Geophys. Geosyst. 16. http://dx.doi.org/10.1002/2014GC005706.

Liu, K.H., Gao, S.S., 2011. Estimation of the depth of anisotropy using spatial coherency of shear-wave splitting parameters. Bull. Seismol. Soc. Am. 101, 2153–2161. http://dx.doi.org/10.1785/0120100258.

Liu, K.H., Gao, S.S., 2013. Making reliable shear-wave splitting measurements. Bull. Seismol. Soc. Am. 103, 2680–2693. http://dx.doi.org/10.1785/0120120355.

Liu, K.H., Gao, S.S., Gao, Y., Wu, J., 2008. Shear wave splitting and mantle flow associated with the deflected slab beneath northeast Asia. J. Geophys. Res. 113, B01305. http://dx.doi.org/10.1029/2007JB005178.

Liu, K.H., Elsheikh, A., Lemnifi, A., Purevsuren, U., Ray, M., Refayee, H., Yang, B., Yu, Y., Gao, S.S., 2014. A uniform database of teleseismic shear wave splitting measurements for the western and central United States. Geochem. Geophys. Geosyst. 15, 2075–2085. http://dx.doi.org/10.1002/2014GC005267.

Mainprice, D., Barruol, G., Ismail, W.B., 2000. The seismic anisotropy of the Earth's mantle: from single crystal to polycrystal. In: Karato, S.-I., Forte, A., Liebermann, R., Masters, G., Stixrude, L. (Eds.), Earth's Deep Interior: Mineral Physics and Tomography from the Atomic to the Global Scale. AGU, Washington, DC.

Malservisi, R., Hugentobler, U., Wonnacott, R., Hackl, M., 2013. How rigid is a rigid plate? Geodetic constraint from the TrigNet CGPS network, South Africa. Geophys. J. Int. 192, 918–928. http://dx.doi.org/10.1093/gji/ggs081.

McCourt, S., Armstrong, R.A., Jelsma, H., Mapeo, R.B.M., 2013. New U–Pb SHRIMP ages from the Lubango region, SW Angola: insights into the Palaeoproterozoic evolution of the Angolan Shield, southern Congo craton, Africa. J. Geol. Soc. (Lond.) 170, 353–363. http://dx.doi.org/10.1144/jgs2012-059.

Miensopust, M.P., Jones, A.G., Muller, M.R., Garcia, X., Evans, R.L., 2011. Lithospheric structures and Precambrian terrane boundaries in northeastern Botswana revealed through magnetotelluric profiling as part of the southern African magnetotelluric experiment. J. Geophys. Res. 116, B02401. http://dx.doi.org/10.1029/2010JB007740.

Niu, F., Li, J., 2011. Component azimuths of the CEArray stations estimated from P-wave particle motion. Earthq. Sci. 24, 3–13. http://dx.doi.org/10.1007/s11589-011-0764-8.

O'Neill, C.J., Kobussen, A., Lenardic, A., 2010. The mechanics of continental lithosphere–asthenosphere coupling. Lithos 120, 55–62. http://dx.doi.org/10.1016/j.lithos.2010.07.008.

Refayee, H.A., Yang, B.B., Liu, K.H., Gao, S.S., 2014. Mantle flow and lithosphere–asthenosphere coupling beneath the southwestern edge of the North American craton: constraints from shear-wave splitting measurements. Earth Planet. Sci. Lett. 402, 209–220. http://dx.doi.org/10.1016/j.epsl.2013.01.031.

Ritsema, J., Ni, S., Helmberger, D.V., Crotwell, H.P., 1998. Evidence for strong shear velocity reductions and velocity gradients in the lower mantle beneath Africa. Geophys. Res. Lett. 25, 4245–4248. http://dx.doi.org/10.1029/1998GL900127.

Sandvol, E., Ni, J., Ozalaybey, S., Schlue, J., 1992. Shear-wave splitting in the Rio Grande Rift. Geophys. Res. Lett. 19, 2337–2340. http://dx.doi.org/10.1029/92GL02715.

Sengor, A.M., Burke, K., 1978. Relative timing of rifting and volcanism on Earth and its tectonic implications. Geophys. Res. Lett. 5, 419–421. http://dx.doi.org/10.1029/GL005i006p00419.

Silver, P.G., 1996. Seismic anisotropy beneath the continents: probing the depths of geology. Annu. Rev. Earth Planet. Sci. 24, 385–432.

Silver, P.G., Chan, W.W., 1991. Shear wave splitting and subcontinental mantle deformation. J. Geophys. Res. 96, 16,429–16,454.

Silver, P.G., Savage, M., 1994. The interpretation of shear-wave splitting parameters in the presence of two anisotropic layers. Geophys. J. Int. 119, 949–963. http://dx.doi.org/10.1111/j.1365-246X.1994.tb04027.x.

Silver, P.G., Gao, S.S., Liu, K.H., 2001. Mantle deformation beneath southern Africa. Geophys. Res. Lett. 28, 2493–2496. http://dx.doi.org/10.1029/2000GL012696.

Vauchez, A., Barruol, G., Tommasi, A., 1997. Why do continents break-up parallel to ancient orogenic belts? Terra Nova 9, 62–66. http://dx.doi.org/10.1111/j.1365-3121.1997.tb00003.x.

Vinnik, L.P., Green, R.W.E., Nicolaysen, L.O., 1996. Seismic constraints on dynamics of the mantle of the Kaapvaal craton. Phys. Earth Planet. Inter. 95, 139–151. http://dx.doi.org/10.1016/0031-9201(95)03123-5.

Vinnik, L., Kiselev, S., Weber, M., Oreshin, S., Makeyeva, L., 2012. Frozen and active seismic anisotropy beneath southern Africa. Geophys. Res. Lett. 39, L08301. http://dx.doi.org/10.1029/2012GL051326.

Yu, Y., Liu, K.H., Moidaki, M., Reed, C.A., Gao, S.S., 2015. No thermal anomalies in the mantle transition zone beneath an incipient continental rift: evidence from the first receiver function study across the Okavango Rift Zone, Botswana. Geophys. J. Int. 202, 1407–1418. http://dx.doi.org/10.1093/gji/ggv229.